PHILOSOPHICAL TRANSACTIONS A

rsta.royalsocietypublishing.org

Research

Cite this article: Schönhardt A, Nau D, Bauer C, Christ A, Gräbeldinger H, Giessen H. 2017 Phase-resolved pulse propagation through metallic photonic crystal slabs: plasmonic slow light. *Phil. Trans. R. Soc. A* **375**: 20160065. http://dx.doi.org/10.1098/rsta.2016.0065

Accepted: 19 December 2016

One contribution of 15 to a theme issue 'New horizons for nanophotonics'.

Subject Areas:
optics

Keywords:
plasmonics, slow light, Fano resonance

Author for correspondence:
Harald Giessen
e-mail: h.giessen@pi4.uni-stuttgart.de

Phase-resolved pulse propagation through metallic photonic crystal slabs: plasmonic slow light

Anja Schönhardt[1], Dietmar Nau[1], Christina Bauer[2], André Christ[2], Hedi Gräbeldinger[3] and Harald Giessen[3]

[1]Institute of Applied Physics, University of Bonn, Bonn, Germany
[2]Max-Planck Institute for Solid State Research, Stuttgart, Germany
[3]4th Physics Institute, University of Stuttgart, Stuttgart, Germany

We characterized the electromagnetic field of ultra-short laser pulses after propagation through metallic photonic crystal structures featuring photonic and plasmonic resonances. The complete pulse information, i.e. the envelope and phase of the electromagnetic field, was measured using the technique of cross-correlation frequency resolved optical gating. In good agreement, measurements and scattering matrix simulations show a dispersive behaviour of the spectral phase at the position of the resonances. Asymmetric Fano-type resonances go along with asymmetric phase characteristics. Furthermore, the spectral phase is used to calculate the dispersion of the sample and possible applications in dispersion compensation are investigated. Group refractive indices of 700 and 70 and group delay dispersion values of 90 000 fs^2 and 5000 fs^2 are achieved in transverse electric and transverse magnetic polarization, respectively. The behaviour of extinction and spectral phase can be understood from an intuitive model using the complex transmission amplitude. An associated depiction in the complex plane is a useful approach in this context. This method promises to be valuable also in photonic crystal and filter design, for example, with regards to the symmetrization of the resonances.

This article is part of the themed issue 'New horizons for nanophotonics'.

THE ROYAL SOCIETY
PUBLISHING

1. Introduction

The subject of light transmission through resonant structures has captured the attention of many scientists lately. Slow light [1,2], propagation on excitonic resonances [3], reduced propagation velocity in doped crystals [4] and photorefractives [5] and broadband slow light in surface-plasmon structures [6] have advanced the general knowledge of the interaction of propagating electromagnetic waves with resonant materials [7]. Metallo-dielectric photonic crystal slabs consisting of regular arrays of gold nanoparticles and an underlying waveguide film exhibit a variety of non-trivial and interesting linear [8,9] and nonlinear [10] optical properties. These structures consist of gold nanoparticle or nanowire gratings with a constant period of the order of the wavelength of visible light. In this work, we concentrate on the case of nanowire gratings with a dielectric waveguide below. Using a propagation direction perpendicular to the planes of the layered structure, two resonances can be excited in the sample depending on the polarization of the incident light. These resonances are the particle plasmon resonance in the single gold nanowires and a waveguide mode in the waveguide film. While the latter is excited in either polarization direction, the plasmon is only present for illumination by transverse magnetic (TM) polarized light (figure 1), i.e. by light polarized perpendicular to the grating lines. In this case, the coupling of the waveguide mode and the plasmon resonance leads to the formation of a new quasi-particle, the so-called particle-plasmon-waveguide-polariton [11]. The extinction spectrum of this polariton exhibits two resonance peaks, corresponding to the two polariton branches. These peaks are separated by a region of enhanced transmission [8]. The situation is an example of electromagnetically induced transparency (EIT) [12,13]. The particular situation in our case does not require two laser beams or nonlinear effects, but rather resembles coherent population trapping with Fano-shaped resonances [14]. It was previously shown that EIT systems can generate slow light down to $c/10\,000$ [1,5,15]. In our investigations, we were interested in the complete optical information of the transmitted laser pulse. Therefore, in addition to the magnitude, the phase of the transmitted electric field had to be measured. Knowledge of the phase information greatly adds to the understanding of the physical processes involved. Our presented method as well as the analysis, the simulation of the results and the modelling of the data provides a recipe that is applicable to Fano- and EIT-type systems in solid-state physics in general. Plasmonic Fano systems have gained a lot of interest in the last few years [16,17]. A recent theoretical suggestion of how to realize EIT in metamaterials [13] also implied slow light, and our method can give the means to examine this situation experimentally. A first attempt was made by Urbas and co-workers, where propagation through magnetic resonant metamaterials was measured [18].

Furthermore, the phase and its wavelength dependence reveal valuable information about the dispersion of the traversed medium. From the spectral phase, we calculate the group delay dispersion (GDD). This is a crucial parameter to describe the dispersion, not only of a material, but also of a specific device. As dispersion appears in any material that is used in optical systems, a strong need for various dispersion compensating elements exists. Especially, if this compensation can be achieved on a small spatial scale and with low losses, such an element would be of multifunctional use, e.g. in laser cavities and optical transmission networks. Here, we examine certain samples and estimate their possible application as GDD compensators (§6).

The extinction and phase behaviour of the transmitted light through such photonic crystal slabs can be theoretically calculated by the scattering matrix (S-matrix) method [19]. This theory allows us to calculate the electromagnetic field at any position along the sample layers and for each polarization direction. We compare our experimental results to such S-matrix calculations in §§3b and 4. In addition, we present a plain and intuitive physical model to explain the results of experiment and theory. Such a basic and descriptive model can help to gain immediate and intuitive insight into the sample properties. This is especially interesting for a description of plasmonic crystals. In the case of metamaterials, this model could serve as a simple and intuitive way for the immediate simulation of dielectric functions and dispersion properties of such plasmonic materials [20,21]. Additionally, our

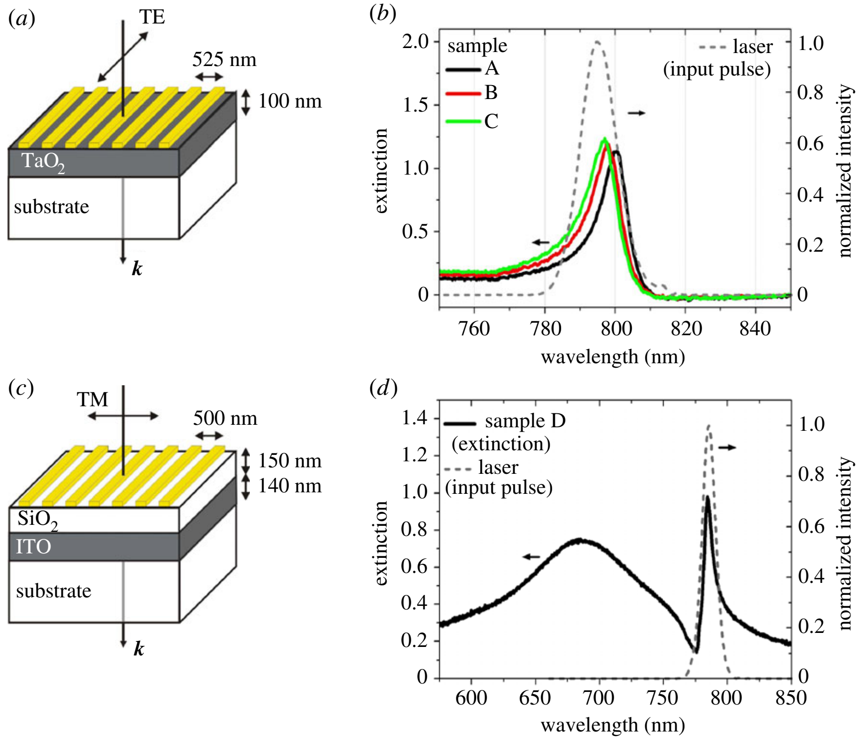

Figure 1. Sample configuration (*a*) and measured extinction curves (*b*) for three slightly different samples (samples A, B and C) in TE polarization. (*c*) The sample design for D and (*d*) the measured extinction spectrum for TM polarization. Different samples (*a*) and (*c*) were chosen to be suitable for the respective situations (see text). The waveguiding layer is coloured grey in both cases. Additionally, in (*b*) and (*d*) the respective input pulse spectra are shown. (Online version in colour.)

model aids the modelling even in the case of nonlinear properties of such plasmonic crystals [22].

2. Sample description and experimental set-up

The photonic crystal slabs analysed here were manufactured by electron beam lithography as in [8] and their geometry is shown in figure 1*a*,*c*. The gold nanowires had a height between 15 and 20 nm and a width of about 150 nm. They were deposited with a period of 525 nm on a 100 nm thick waveguide film (TaO_2). A very thin layer of 10 nm indium–tin oxide (ITO) between the gold lines and the waveguide (not shown in the figure) was necessary for fabrication reasons. The three samples A, B and C were investigated in transverse electric (TE) polarization and, while being nominally identical, they differ in the spectral position of the waveguide mode resonance due to slightly varying values for width and height of the gold wires. This leads to a difference in the spectral detuning of this resonance with respect to the laser input pulse used in the propagation experiments.

Sample D shown in figure 1*c* was used for measurements in TM polarization and its geometry was similar to the description above. The waveguide layer consisted of 140 nm ITO and the gold nanowires were deposited on top of a 150 nm thick SiO_2 spacer layer on top of the ITO. This spacer layer does not change the fundamental physics involved in the following discussions but has an important influence on the coupling strength between the two quasi-particles and the coupling efficiency of the grating. Because of the greater distance between the gold grating and the waveguide layer their coupling is reduced, which results in a longer lifetime of the waveguide mode and therefore a reduced spectral width. This is accompanied by a reduced

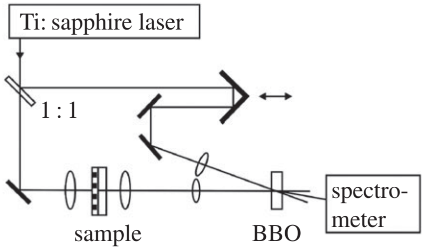

Figure 2. Experimental set-up for the XFROG measurements where TE and TM polarization was achieved by sample rotation.

spectral width of the transmission maximum between the two resonances in TM polarization. As the spectral width of the whole system of the particle plasmon waveguide mode polariton is too broad to be measured with the employed Ti:sapphire laser, only part of it can be covered by the measurement (see §4). In the case of sample D, the covered spectral region contains one polariton branch completely and the region of low extinction between the polariton branches, which was not possible with samples A, B and C. These three samples, however, show a very high extinction in TE polarization, causing strong effects on the transmitted pulse. In this way, suitable samples were chosen for either polarization direction.

Before the phase measurements were performed, we analysed the extinction ($-\ln(T)$, $T =$ transmission) of transmitted white light, combining all losses in the sample such as reflection, absorption and scattering, in order to characterize our samples. The resonances excited in a sample appear as extinction maxima in the spectrum (figure 1*b*,*d*).

Cross-correlation frequency resolved optical gating (XFROG) was then used to characterize the transmitted femtosecond laser pulses in the spectral and temporal domains as described in [23,24]. Alternative approaches have been applied by Dogariu *et al.* [25]. XFROG allows for the retrieval of the intensity as well as the phase behaviour of short laser pulses. The experimental set-up is shown in figure 2. For the measurements, a Ti:sapphire laser was used with a pulse duration of 90 fs and a spectral width of 12 nm around 795 nm or 785 nm (figure 1). The laser beam is split by a 1 : 1 beamsplitter into two equivalent parts of which one passes through the sample (sample arm) and the other one remains unaltered (reference arm). The two then unequal pulses are focused into the centre of a 100 µm thin BBO crystal, yielding a sum frequency signal of the two pulses in the case of an overlap in time and space. The position of the retroreflector controls the time overlap. As the properties of the Ti:sapphire laser pulse have to be known as precisely as possible, we also measured the autocorrelation of the pulse with this set-up by guiding the pulse in the sample arm around the sample.

The FROG trace of the original Ti:sapphire pulse is shown in figure 3*a*. Apart from a slight irregularity at higher wavelengths, this FROG trace is quite symmetric. This pulse was used to examine the properties of samples A, B and C in TE polarization. For the experiments on sample D in TM polarization, the laser pulse was tuned to lower wavelengths around 785 nm. In the set-up, the two different polarization directions were achieved by rotating the sample around the beam axis.

3. Results for transverse electric polarization

(a) Cross-correlation frequency resolved optical gating measurements and retrievals of E-field

The XFROG traces taken after propagation through samples A, B and C are shown in figure 3*b*–*d*, respectively. By travelling through the sample arm, the pulse gains additional chirp due to the dispersive materials of the microscope objectives and the sample substrate. This results in slight temporal broadening and a tilt of the spectrogram. Apart from this, the XFROG traces

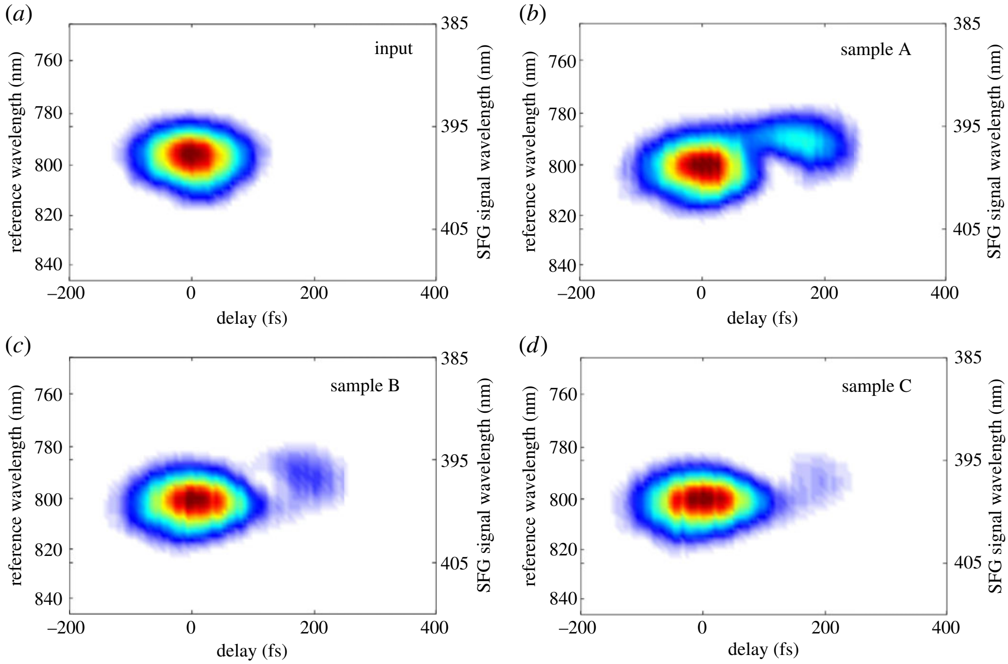

Figure 3. Spectrogram (*a*) shows the FROG trace of the input laser pulse. After propagation through samples A, B and C, the pulse is split into two pulses as can be clearly seen in (*b–d*), respectively. (Online version in colour.)

show distinct differences compared with the FROG trace. The pulse splits into two separate pulses in time with a spacing of about 180 fs. From these spectrograms, the electric field in dependence of time and wavelength is calculated by using the FROG and XFROG algorithms [24].

The transmitted electric field obtained from these XFROG traces is shown in figure 4 with respect to the wavelength (figure 4*a*–*c*) and time (figure 4*d*–*f*). The waveguide resonance appears in the transmitted spectrum as a pronounced intensity minimum. This minimum shifts to lower wavelengths from sample A to C, according to the spectral position of the resonance. The phase ϕ is calculated from two measurements, one having the laser pulse propagating through the complete sample, and one where the pulse traverses the sample next to the gold lines, the so-called substrate measurement. This is needed to subtract effects caused by the substrate. This phase ϕ is defined as the phase of the transmission amplitude t of the electrical field, $t = |t| \exp(\mathrm{i}\phi)$, as also used later in §5. Here we always plot the phase difference $\phi_{\mathrm{Sample}} - \phi_{\mathrm{Substrate}}$. Exactly at the position of the waveguide mode, the spectral phase shows a dispersive behaviour with a phase jump of about $\pi/2$.

In the time domain, the laser pulse is clearly split into two separate pulses as expected from the spectrogram. This phenomenon can be assigned to the beating between the two spectrally disjoint pulse parts. For beating phenomena, the phase is expected to display a phase jump of π at the position between the maxima of the field envelope. These phase jumps are clearly visible in the experimental results and amount to values between $\pi/2$ and π here.

(b) Scattering matrix simulations

In the following, the scattering matrix approach [19,26,27] is used to interpret our experimental results. Within this theory, electromagnetic fields propagating in slab structures can be calculated. The dielectric functions of the considered slabs are restricted to be either homogeneous or periodic, which is the case for our samples. The geometry of the sample, which is known from the fabrication itself and measurements with a scanning electron microscope (SEM), enters into

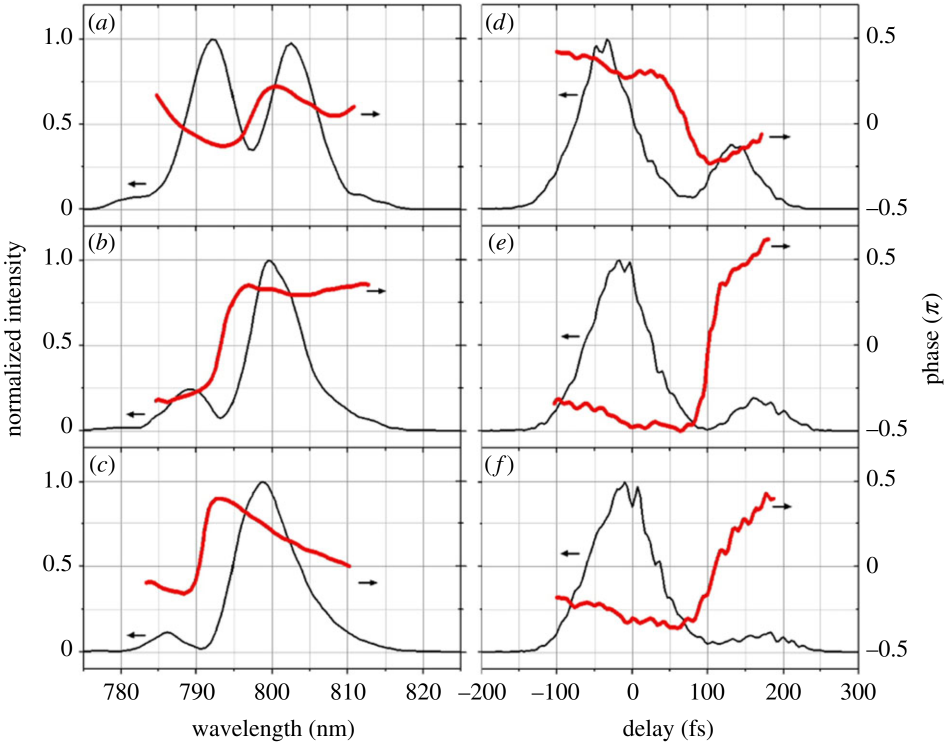

Figure 4. Spectral (*a–c*) and temporal (*d–f*) intensity and phase ($\phi_{\text{Sample}} - \phi_{\text{Sub}}$) of the transmitted Ti: sapphire laser pulse measured for sample A (*a*,*d*), B (*b*,*e*) and C (*c*,*f*). (Online version in colour.)

the computation. Only the height of the gold structure was not accessible here and, therefore, its value was adjusted for the calculation. However, the height lies in the region of values that was intended in the fabrication. From the S-matrix calculation, we obtained the extinction and the spectral phase of the transmitted light field. These results are compared with our experimental data in figure 5 for the three samples A, B and C. The graphs show very good agreement between theory and experiment. The waveguide resonances seen in the experiment are well reproduced by the theory. They appear spectrally at the same position and have the asymmetric line shape of Fano resonances [28,29] as in the experimental results. Additionally, the phase performs the same evolution: at the position of the resonance a phase jump occurs. This jump is not abrupt, but rather has a dispersive behaviour as discussed in §3a. The height of the phase jump as well as its form and spectral position are in good agreement with the experimental results. Furthermore, an asymmetry of the phase evolution around the resonance frequency is visible. The positive phase bend on the steeper side (higher wavelengths) of the Fano resonance is more pronounced than the phase minimum on the lower side. This can also be seen in the measurements, especially well in figure 5*c*. Slight deviations at the side regions are probably due to less laser intensity and thus larger uncertainties. The phase behaviour in figure 5*b*, for example, differs somewhat in that the curve does not return to zero at the sides of the resonance. But apart from this, the S-matrix results support our experimental results very well.

4. Cross-correlation frequency resolved optical gating and theoretical results for transverse magnetic polarization

In this section, experiments are presented for sample D (figure 1) in TM polarization and compared with theoretical S-matrix results. The Ti:sapphire laser pulse, which was used to

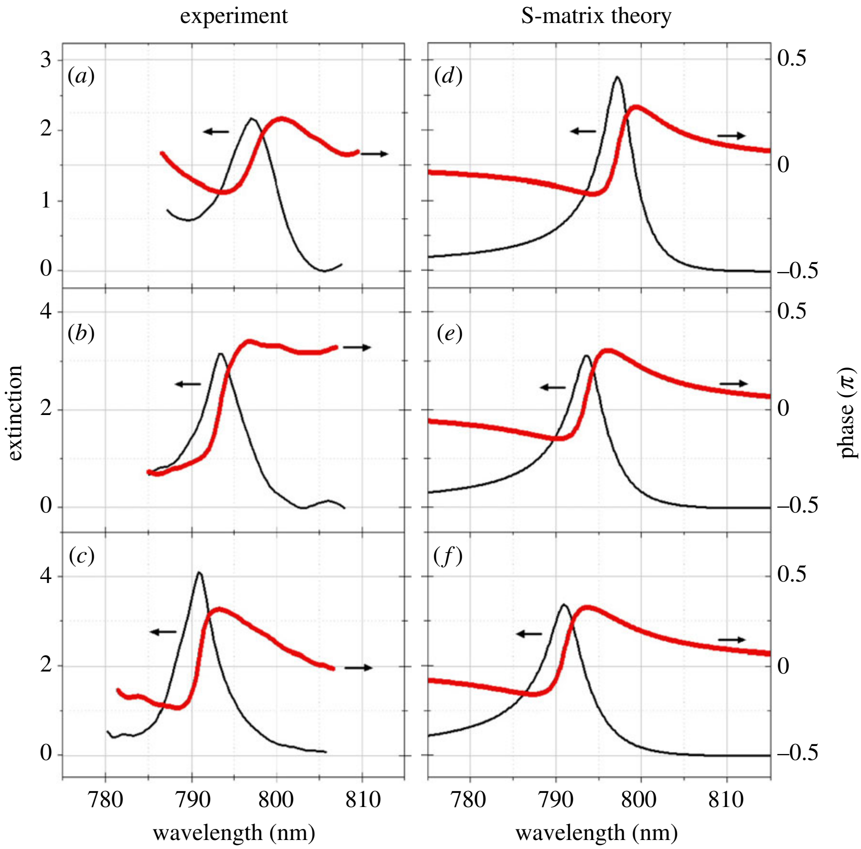

Figure 5. Comparison between experimental results (*a–c*) of samples A, B and C and the results from S-matrix theory (*d–f*) for the extinction and phase. (Online version in colour.)

investigate the sample properties here, was spectrally less broad than the extinction spectrum of the coupled quasi-particle system. Therefore, only part of the spectrum could be covered by the phase-resolved measurement. This spectral region mainly contains the low energy polariton and part of the extinction minimum between the two resonances. As explained in §2, the TM measurements were performed using sample D because this sample exhibits narrower features than samples A, B and C. The latter three samples could not be analysed by the present Ti:sapphire laser in TM polarization, but were especially suitable for the TE measurements presented here. In all cases, an even broader laser spectrum could further improve the quality of the measurements, particularly in TM polarization. The FROG trace of the Ti:sapphire pulse and the XFROG trace of the pulse after propagation through sample D are shown in figure 6*a*,*b*, respectively. The influence of the sample on the laser pulse can be seen directly. Part of the compact laser pulse arrives delayed at the detector with the pulse appearing stretched. This result is similar to the situation in TE polarization, except the effect is less pronounced. The delayed part is not separated from the rest of the pulse.

For completeness and better comparison, the entire extinction spectrum measured by white light transmission (cf. §2) is shown in figure 7 together with the result from S-matrix theory. For the theoretical calculation, several geometrical and material parameters were needed. The applied values for the refractive indices were $\epsilon_{SiO_2} = 2.13$, $\epsilon_{ITO} = 3.8$ [8] and the gold dielectric function was taken from [30]. The substrate had a refractive index of $n = 1.515$. According to SEM measurements, the gold wires were taken to have a width of 140 nm and a height of 20 nm, at a period of 490 nm.

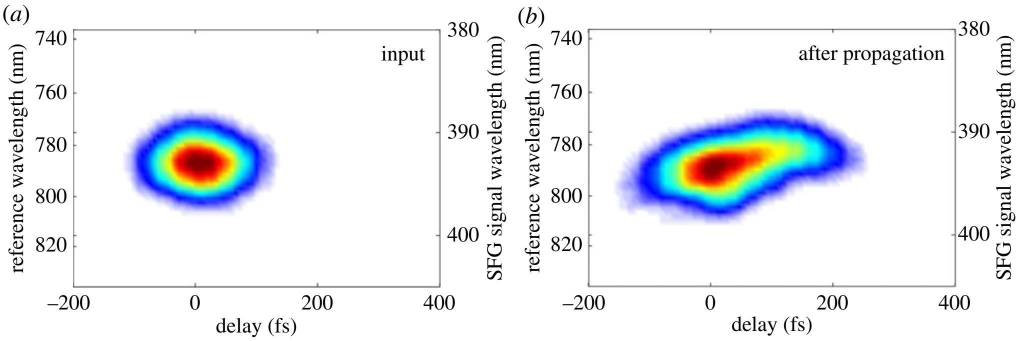

Figure 6. (X)FROG traces of the input Ti:sapphire pulse (*a*) and of the pulse after propagation through sample D in TM polarization (*b*). (Online version in colour.)

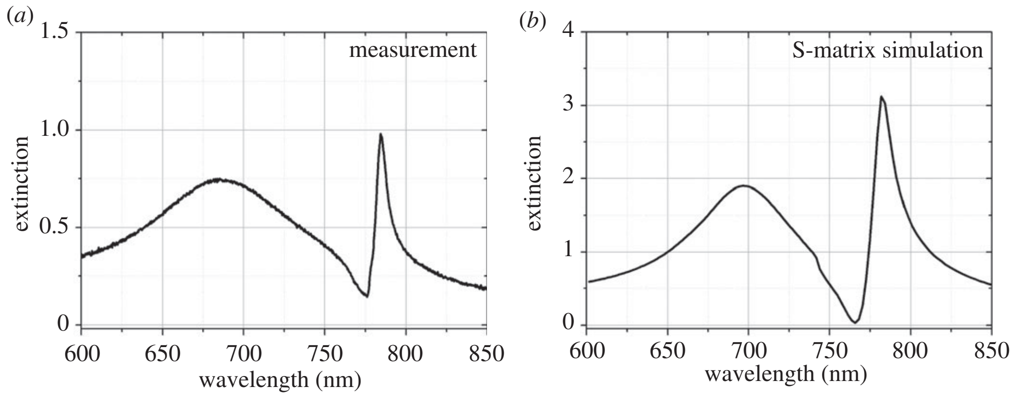

Figure 7. Extinction spectrum measured for sample D by white light transmission (*a*) and calculated by S-matrix theory (*b*). Good agreement between measurement and theory is achieved.

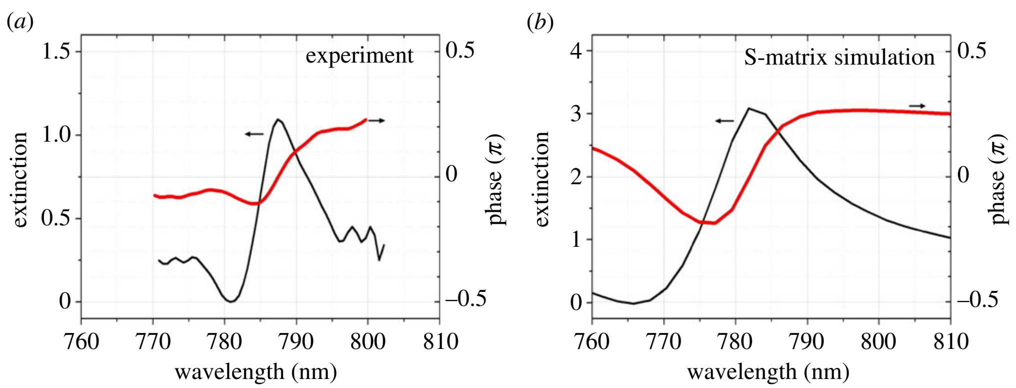

Figure 8. Extinction and phase of the transmitted laser pulse obtained from the experiment (*a*) and S-matrix theory (*b*). Owing to bandwidth constraints of the Ti:sapphire laser only the low energy polariton was covered by the measurement. (Online version in colour.)

The retrieval of the electric field from the phase-resolved XFROG measurement yields the result shown in figure 8 for the extinction and the spectral phase. The polariton resonance appears as an extinction maximum and the phase exhibits a jump at the centre of the resonance. This qualitative behaviour is already known from TE polarization (§3). The phase has a dispersive shape and the magnitude of the jump here amounts to about 0.3π. This is slightly less than the value previously obtained. For direct comparison, the results from S-matrix calculations are shown in the same figure (figure 8*b*); only the sector of the spectrum covered by the measurement is shown. Figure 12*a* shows a broader spectral range of the same polaritonic system.

5. Intuitive coupled oscillator model

The S-matrix method is well suited to describe the pulse propagation through a slab structure. However, it is helpful to explain the processes involved in a more intuitive way, especially when it comes to the properties of the polaritonic quasi-particles. Therefore, we strive to find a model that allows for the calculation and visualization of the spectra for extinction and phase. At the same time, we would like to understand the relation between the quasi-particles and the origin of the asymmetry in the extinction and phase spectra.

An intuitive model was proposed by Fan *et al.* [31] for a quantitative explanation of resonance line shapes. This model was used for transmission through lossless photonic crystal slabs. As discussed there, we have an interference phenomenon between two different pathways—the direct transmission and the indirect path via the excitation of a resonance in the sample. Here, we want to modify this model for our case and for the experimental and theoretical results in real samples.

The model can be extended to contain both cases—the transmission for TE polarization with exclusive excitation of a waveguide mode as well as for TM polarization with excitation of a particle-plasmon-waveguide-mode-polariton. These quasi-particles can be modelled as interfering Lorentz oscillators. For this purpose, the transmission amplitudes of the excitations are added to a constant which describes the direct transmission. The resulting transmission amplitude t characterizes the coupled system with interference between all channels:

$$t(\omega) = \left(1 + \frac{-\Gamma_{\mathrm{WG}}|f_{\mathrm{WG}}|}{\hbar\omega - E_{\mathrm{WG}} + \mathrm{i}\Gamma_{\mathrm{WG}}} \cdot \mathrm{e}^{\mathrm{i}\alpha_{\mathrm{WG}}} + \frac{-\Gamma_{\mathrm{PL}}|f_{\mathrm{PL}}|}{\hbar\omega - E_{\mathrm{PL}} + \mathrm{i}\Gamma_{\mathrm{PL}}} \cdot \mathrm{e}^{\mathrm{i}\alpha_{\mathrm{PL}}}\right) \cdot \mathrm{e}^{\mathrm{i}\varphi_0}. \tag{5.1}$$

The index WG in the above equation is related to the waveguide mode, whereas PL describes the parameters associated with the particle plasmon. E is the resonance energy, Γ is the spectral width and f is the oscillator strength of the respective resonance. If now only one of the two resonances is excited, i.e. the TE mode or an independent plasmon resonance, the respective oscillator strength of the other term is set to zero. By φ_0 an additional phase is introduced, accounting for some overall propagation phase. The angle α is in general the phase shift between the directly transmitted light and the light emitted from the resonance. In the case of an undisturbed Lorentz resonance, α obtains the exact value of $\pi/2$. Here, with neighbouring resonances and additional scattering phases, the value can differ from $\pi/2$. We emphasize that this difference is the crucial point that makes the simulation of asymmetric Fano resonances on the basis of mere Lorentz resonances possible here. No further changes or adjustable parameters are needed. A similar relation to equation (5.1) was also presented in [32], where the transmission amplitude was derived directly from a fundamental scattering matrix theory approach. In difference to [32], we keep the constant 1 in the sum fixed to account for the directly transmitted light. Additionally, we have introduced the explicit scattering phase within the parameters α as explained earlier.

As t is a complex number, it can be written as $t = |t|\exp(\mathrm{i}\phi)$, from which we calculate the extinction $-\ln(T) = -\ln(|t|^2)$ as well as the phase behaviour $\phi(\omega)$ of a transmitted electromagnetic field.

(a) Model results for transverse electric polarization

The extinction and spectral phase of the transmission amplitude for a pure Lorentz (LO) case are shown in figure 9*a*. The parameters are $\lambda_{\mathrm{LO}} = hc/E_{\mathrm{LO}} = 800\,\mathrm{nm}$, $\Gamma_{\mathrm{LO}} = 10\,\mathrm{meV}$, $|f_{\mathrm{LO}}| = 0.8$, $\varphi_0 = 0$

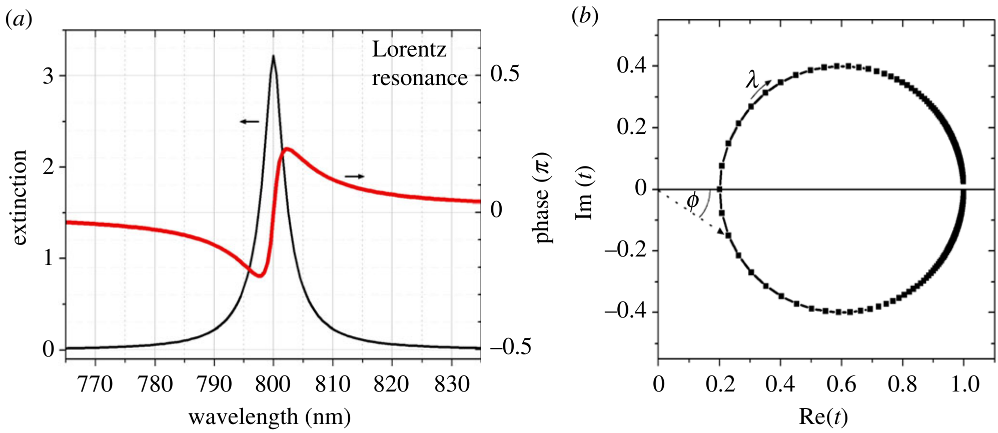

Figure 9. Extinction and phase of the transmission amplitude through a pure Lorentz resonance (*a*) and the associated complex plot of the same transmission amplitude (*b*). The length of the dashed arrow corresponds to the transmission, and the angle φ denotes the phase when changing the wavelength along the circle. (Online version in colour.)

and $\alpha_{LO} = \pi/2$. Both curves show a clear symmetry around the spectral position of the resonance. In figure 9*b*, the same transmission amplitude is plotted in the complex plane, which proves to be a very useful description that reveals the magnitude of the transmission and the phase simultaneously. As the frequency ω changes, the transmission amplitude performs the circular trajectory shown here. For far off-resonant wavelengths, the transmission amplitude amounts to 1 and the phases have to be the same, as both parts of the spectrum are not influenced by the resonance. In this diagram, it is very instructive as to which physical variables change if certain parameters vary. We will, therefore, subsequently use this construction. For the Lorentz case, the above mentioned symmetry about the real axis also becomes very clear in the complex plane. The circle is centred on the real axis, beginning and ending at the same point $t = 1$ for zero and infinite energy.

This symmetry is broken as soon as additional scattering phases change the value of the phase α away from $\pi/2$. This occurs in the case of the excitation of waveguide modes in our sample. Because of the interference between the direct and indirect transmission channels and because of the fact that the indirect transmission exhibits an additional phase, the overall transmission becomes asymmetric. For sample A, the extinction and phase evolutions, as derived by the S-matrix, are again shown in figure 10*a* and directly compared with the result obtained with the oscillator model in figure 10*b*. The parameters used for the model were $|f_{WG}| = 0.8$, $\lambda_{WG} = hc/E_{WG} = 798.5\,\mathrm{nm}$, $\Gamma_{WG} = 10\,\mathrm{meV}$, $\alpha_{WG} = 0.4\pi$ and $\varphi_0 = 0$. The good agreement between the two representations is evident. In figure 10*c*, both results are plotted together in one single complex plane, so that direct comparison is possible. This figure is especially significant as it shows that the trajectory of the transmission amplitude still performs a circle in the complex plane. However, for the S-matrix result, we find an additional phase which causes the rotation about the circle origin. Therefore, the additional phase introduced in equation (5.1) is justified. We demonstrate the usefulness of this concept in §6b.

For two examples (samples A and C) the complex diagram of the measured transmission is presented in figure 11 in direct comparison with the result from the introduced oscillator model. Again, good agreement between our simple model and the experiments is achieved.

(b) Model results for transverse magnetic polarization

The oscillator model presented in the previous section is now employed to describe the behaviour of the quasi-particle system in TM polarization. Two interfering Lorentz oscillators

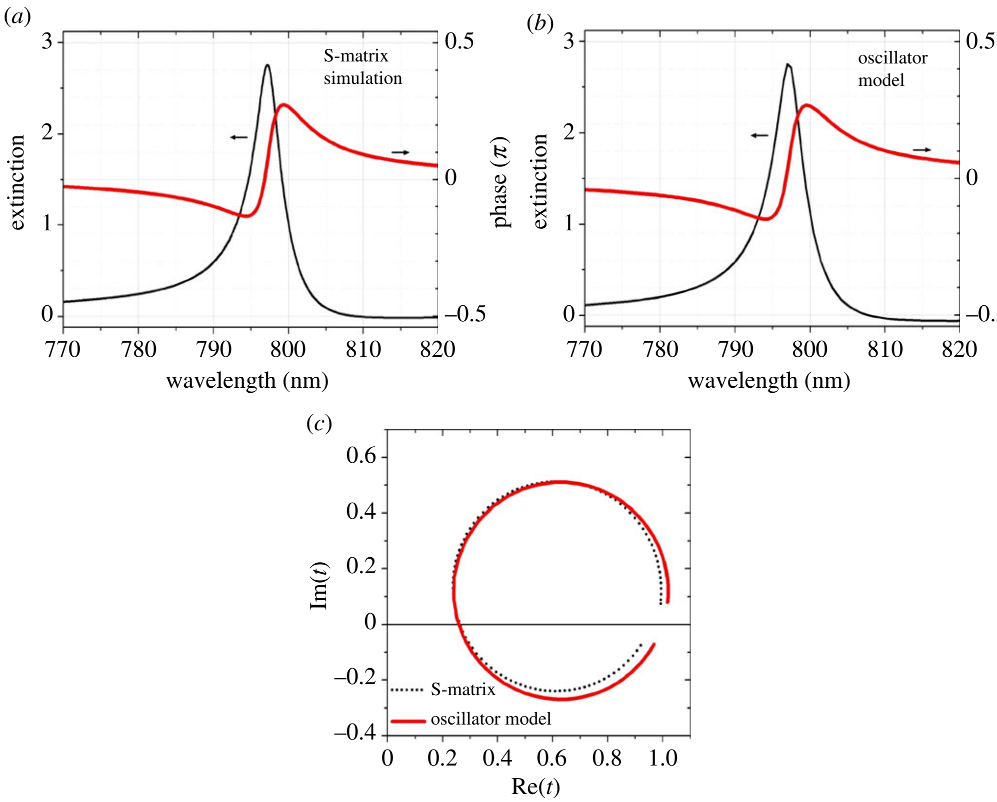

Figure 10. Extinction and phase of the transmission amplitude through sample A calculated by S-matrix theory (*a*), and result for the extinction and phase evolution from the oscillator model (*b*). An additional scattering phase in the model and the interference with the directly transmitted light causes an asymmetry and, therefore, the Fano line shape. Comparison of S-matrix theory and oscillator model result in the complex plane (*c*). (Online version in colour.)

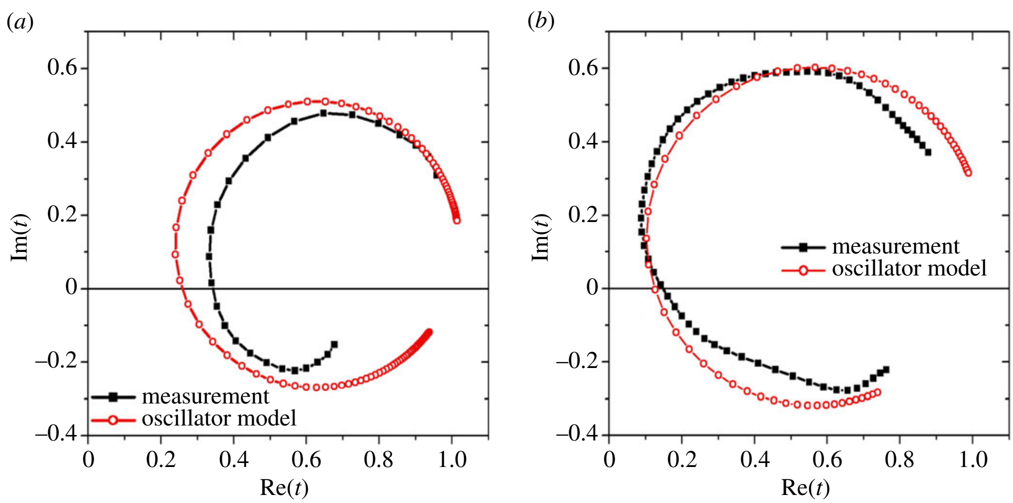

Figure 11. The complex transmission amplitude is shown in the complex plane. Comparison between experimental results and the calculations from the proposed oscillator model for sample A (*a*) and sample C (*b*). (Online version in colour.)

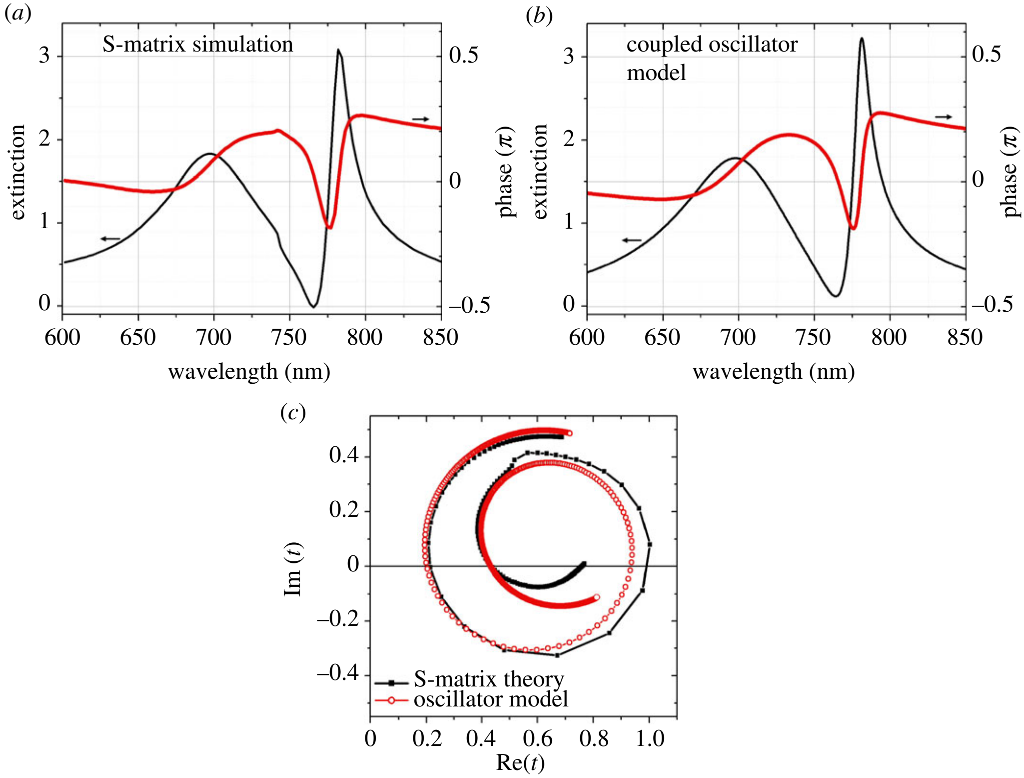

Figure 12. Comparison between S-matrix theory (*a*) and the coupled oscillator model (*b*). The extinction spectra are shown in black, the phase in red. (*c*) Complex diagram of the transmission amplitude for S-matrix calculation (black) and the coupled oscillator model (red). The parameters used for the model calculation are stated in the main text. (Online version in colour.)

with additional scattering phases suffice to produce a transmission amplitude that can very well describe the polariton extinction and also the phase behaviour. In figure 12*a*,*b*, the extinction and phase curves from the S-matrix calculation are compared with these model results. The agreement between the two methods is quite good. The extinction spectrum of the model result shows a clear asymmetry of the two resonance peaks as in the S-matrix theory. Furthermore, the enhanced transmission separating the two polariton branches appears correctly. Although the phase characteristic is rather distorted due to the close-by resonances, the model generates the expected behaviour. The parameters used for the model result were $|f_{\mathrm{WG}}| = 0.83$, $\lambda_{\mathrm{WG}} = hc/E_{\mathrm{WG}} = 772\,\mathrm{nm}$, $\Gamma_{\mathrm{WG}} = 20\,\mathrm{meV}$, $\alpha_{\mathrm{WG}} = \pi$ and $|f_{\mathrm{PL}}| = 0.7$; $\lambda_{\mathrm{PL}} = hc/E_{\mathrm{PL}} = 715\,\mathrm{nm}$, $\Gamma_{\mathrm{PL}} = 210\,\mathrm{meV}$, $\alpha_{\mathrm{PL}} = 0.43\pi$ and $\varphi_0 = 0.06\pi$.

The consistency of the model with the S-matrix calculation is again demonstrated by the depiction in the complex plane (figure 12*c*). Apart from slight deviations in the enhanced transmission region, the two trajectories coincide very well. On the account of the high yet limited accuracy of the S-matrix theory (due to the truncation of an infinite sum of plane waves within the calculation) and the simplicity of the used model, small differences between the two results remain.

Although the given model only uses the transmission amplitudes of pure Lorentz oscillators, the implementation of an overall scattering phase for each excitation results in non-Lorentzian extinction spectra and phase characteristics for waveguide modes and polariton systems in good agreement with the presented measurements and S-matrix theory. Hence, especially the asymmetric Fano line shapes and the enhanced transmission between two polaritons can be generated within this model.

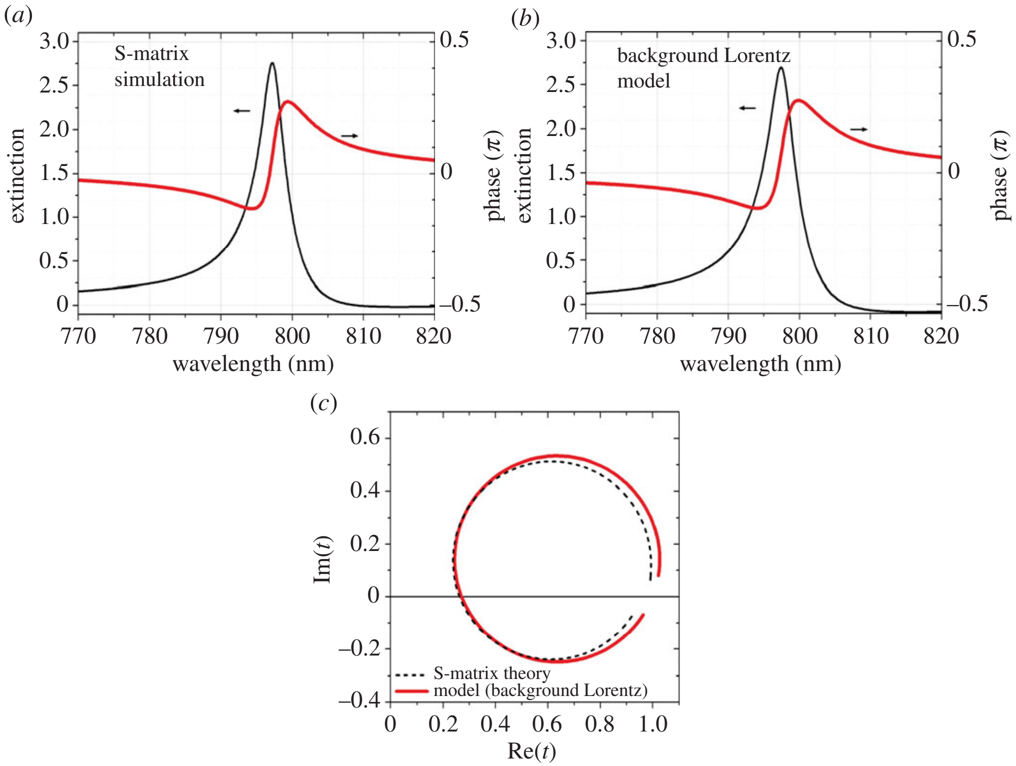

Figure 13. Effective extinction and phase (*b*) from the background Lorentz model after division by the modelled substrate measurement. (*a*) The result from S-matrix theory for comparison. The complex plot (*c*) contains the trajectories for S-matrix theory (red) and the background Lorentz model (black). All figures refer to sample A. (Online version in colour.)

(c) Background Lorentz model for transverse electric polarization

Another reason for the existing asymmetry of the waveguide modes are spectrally detuned higher absorption resonances that influence the spectral region under inspection. Such resonances exist in dielectric materials such as ITO in the UV region [33]. As they are very broad they contribute a constant complex value to the transmission amplitude. In general, we account for substrate influences on the extinction measurement by dividing the transmission through the sample by the transmission through the substrate, which is exactly the same sample without the gold grating. If we model this with the oscillator model and describe the excitations in the glass substrate by another Lorentz resonance in the UV, we can abandon the additional phases and set all values to $\alpha = \pi/2$. The result obtained from this calculation is shown in figure 13.

Figure 13*b* shows the extinction and phase behaviour, while figure 13*c* depicts the result in the complex plane. Strikingly, the transmission amplitude appears again as a rotated circle. So the asymmetry of the observed resonances has two possible physical origins—one being the additional scattering phase obtained by the pulse during the excitation and emission process from the resonance, the other one resulting from higher absorption resonances in the surrounding materials.

6. Applications

(a) Group delay dispersion compensation

In the following, we calculate the dispersion properties of the samples using the retrieved spectral phase ϕ of the transmitted laser pulse. This phase evolution determines directly the magnitude of

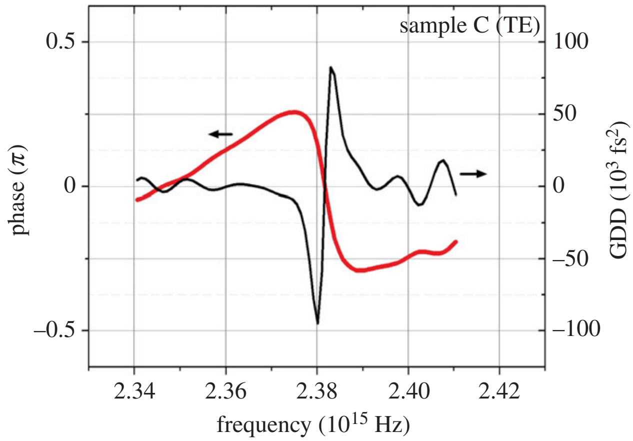

Figure 14. Measurement on sample C in TE polarization: the phase evolution of the transmitted E-field is shown along with the respective GDD curve. (Online version in colour.)

the GDD, D_ϕ, which is defined as

$$D_\phi = \frac{\partial^2 \phi}{\partial \omega^2}. \tag{6.1}$$

This value contains the dispersion information of a certain optical device. In our case, this is the additional dispersion caused by the polariton in the sample and a phase difference $\phi = \phi_{\mathrm{Sample}} - \phi_{\mathrm{Substrate}}$ results. In figure 14, the GDD value is plotted in one single graph together with the phase behaviour for sample C. Obviously, the GDD is very strongly frequency dependent. Far off resonance, D_ϕ takes on very small values and varies around zero. Close to the resonance, where the phase jump occurs, the dispersion starts to fluctuate strongly. At the greatest, the GDD attains high values of up to $\pm 90\,000\,\mathrm{fs}^2$, as illustrated in figure 14 for sample C in TE polarization. This can be compared with the dispersion of 3 m of standard optical fibre (at 800 nm), but is rather achieved only on a length scale of 100 nm (gold line plus waveguide thickness). A potential problem is the non-vanishing extinction close to the resonance. This could make an application in a laser cavity difficult. There might be other applications where small losses are tolerable. However, it would be generally interesting to use a sample in TM polarization at the spectral position between the resonances where the extinction drops to zero. The calculation in figure 15 was performed for sample D in TM polarization at the spectral position of the lower energetic polariton branch. The phase shown in this graph is identical with the one shown in figure 8*b*. In this case, the GDD reaches values up to $\pm 5000\,\mathrm{fs}^2$, which is an order of magnitude less than for the case of sample C in TE polarization. The group index ($n_{\mathrm{gr}} = c/v_{\mathrm{gr}} = c/(L \cdot (\partial\phi/\partial\omega)^{-1})$) at resonance is calculated to be approximately 700 in TE polarization and 70 in TM polarization. These values take into account the film thickness L (waveguide + spacer layer + grating structure) of 130 nm for sample C (TE) and 310 nm for sample D (TM). Considering only the actual thickness of the grating structures (20 nm), the group index amounts to around $n_{\mathrm{gr}} = 4500$ or $n_{\mathrm{gr}} = 1000$ for TE and TM polarization, respectively. The maximum value that the GDD can reach depends crucially on the sample design. At sharper resonances, the phase of the electric field performs the discussed phase jump within a smaller spectral range. Therefore, larger values for the phase curvature can be achieved at narrow resonances. A possible goal could be to design and fabricate a sample featuring a very narrow waveguide resonance coinciding spectrally exactly with the plasmonic resonance. This sample should ideally show a vanishing extinction in TM polarization between the two polariton branches and would be a good starting point for a GDD compensating device with negligible losses. In general, due to sample imperfections, it is difficult to fabricate samples with zero losses.

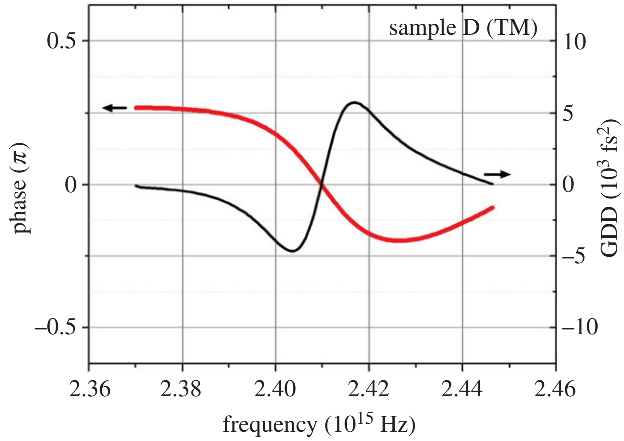

Figure 15. S-matrix theory on sample D in TM polarization showing the phase evolution of the transmitted E-field and the respective GDD curve. (Online version in colour.)

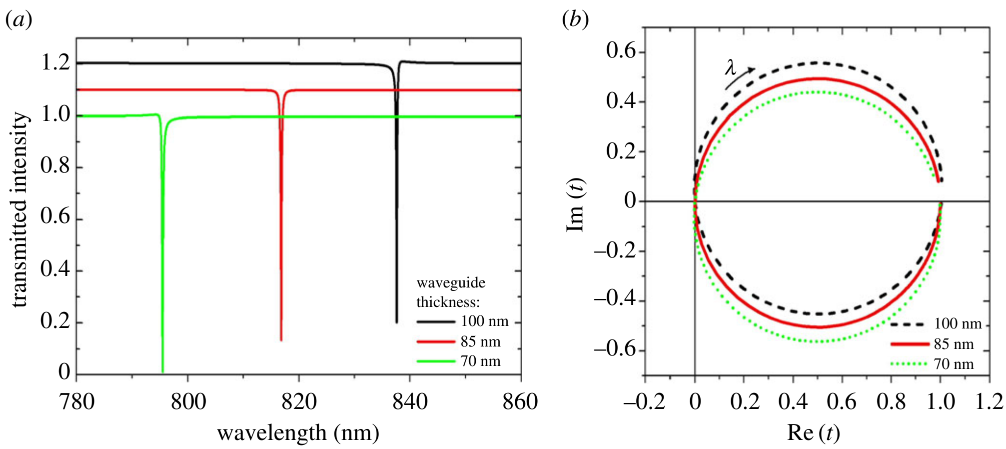

Figure 16. (*a*) Spectral transmission intensity of these structures. Note the symmetric behaviour of the structure with 85 nm waveguide thickness. The curves have been displaced for better visibility by 0.1. (*b*) Complex transmission amplitude of a 15 nm TaO_2 wire grating with 100 nm wide wires and a period of 525 nm on a 70, 85 and 100 nm TaO_2 waveguide film on quartz substrate. The three circles belonging to the different waveguide thicknesses are rotated around $t = 1$ because of the varying scattering phases. (Online version in colour.)

(b) Symmetric filter

We can use the results of §5a for designing transmission filters whose spectral response has been optimized for an especially symmetric shape. The scattering phase rotates the circular transmission amplitude in the complex plane around the origin of the circle at $(\mathrm{Re}(t), \mathrm{Im}(t)) = (1, 0)$. If we could influence the scattering phase by designing the structure appropriately, we would achieve a perfectly symmetric circle with respect to the real axis. This directly implies a symmetric spectral transmission as well as a symmetric phase behaviour around the resonance. The key parameter to modify the scattering phase is the waveguide thickness. If we choose carefully so that we do not reach the cut-off wavelength and do not have multimode propagation either, the scattering phase scales with the waveguide thickness. Figure 16*b* shows the complex transmission amplitudes for three different waveguide thicknesses, which were calculated by scattering matrix theory. The 85 nm thick waveguide shows the most symmetric circle with respect to the real axis, whereas the 100 nm and 70 nm thick waveguides lead to circles rotated above and below the real axis.

Figure 16*a* compares the transmission characteristics of these three different realizations of photonic crystals. Note that we have chosen for simplicity a purely dielectric structure with 15 nm thick and 100 nm wide TaO_2 wires. The concept holds true also for metallic structures; however, the achievable filter linewidth is narrower in the purely dielectric structure. The sample with the 70 nm waveguide exhibits a dispersive lineshape on the low wavelength side, followed by a sharp dip and a somewhat asymmetric shoulder on the long wavelength side. The sample with the 85 nm waveguide displays perfectly symmetric behaviour, whereas the sample with the 100 nm waveguide behaves just the opposite of the 70 nm sample.

Therefore, the complex transmission diagram is quite useful for optimization of the design of optical filter structures.

7. Conclusion

We have examined the propagation of ultrashort laser pulses through metallo-dielectric photonic crystal slabs by performing phase-resolved XFROG measurements. The experimental results agree very well with S-matrix simulations and show a strong influence of the polaritonic sample characteristics on the phase of the transmitted laser pulse. The temporal phase performs a phase jump of about $\pi/2$ to π, while the spectral phase shows a dispersive behaviour and a central jump height of about $\pi/2$. These features occur at the positions of the excitations in the sample. Furthermore, the spectral phase exhibits asymmetries, contrary to a pure antisymmetric phase characteristic for a Lorentz resonance about the resonance frequency. This goes along with the well-known asymmetric line shape of the Fano-shaped waveguide mode resonance, which resembles an EIT-like situation in the case of TM polarization. The results from experiment and theory can be modelled and explained on a physical basis via a transmission amplitude containing mere Lorentz resonances with additional scattering phases. Including a Lorentz resonance to account for excitations in the background material at UV wavelengths also leads to the desired asymmetry. The depiction of the transmission amplitude in the complex plane yields deeper insight into the nature of the resonances. As theory and model results show, the transmission amplitude performs a circle in the complex plane, and this circle appears rotated with respect to the circle origin. This fact is due to the scattering phases and neighbouring resonances. The influence of the different parameters on the appearance of the complex plot gives useful hints for the design of optical elements.

The samples show very high values around 90 000 fs^2 for the GDD, which is a prerequisite for a possible applications in dispersion compensation. Although the GDD curves are rather fluctuating, the samples could be employed in certain wavelength regions and in situations where some losses are tolerable. Group refractive indices of 700 and 70 were determined for TE and TM polarization, respectively, which are substantially larger than the ones expected in the metamaterial case. These values are remarkable, given that the sample structure is only of the order of 100 nm thick. This work was conceived in A.S.'s diploma thesis (University of Bonn, 2005).

Symmetrizing the spectral line shapes of the resonances for device applications was aided by using the simple and intuitive design features of the presented complex transmission model in the complex plane. In fact, we can symmetrize the observed spectral waveguide resonances by choosing the thickness of the waveguide layer appropriately.

Competing interests. The authors declare that they have no competing interests.

Funding. Financial support by ERC (Complexplas), DFG (SPP1113 and FOR557) and BMBF (13N8340/1) is gratefully acknowledged.

Acknowledgements. We thank D. Türke, S. Tikhodeev, H. Guo, C. Ropers, M. Stockman and T. Höner for discussions, S. Linden for programming assistance and the teams of R. Langen and K. D. Krause for technical support.

References

1. Hau LV, Harris SE, Dutton Z, Behroozi CH. 1999 Light speed reduction to 17 metres per second in an ultracold atomic gas. *Nature* **397**, 594–598. (doi:10.1038/17561)
2. Yanik MF, Fan S. 2004 Stopping light all optically. *Phys. Rev. Lett.* **92**, 083901. (doi:10.1103/PhysRevLett.92.083901)
3. Nielsen NC, Linden S, Kuhl J, Förstner J, Knorr A, Koch SW, Giessen H. 2001 Coherent nonlinear pulse propagation on a free-exciton resonance in a semiconductor. *Phys. Rev. B* **64**, 245202. (doi:10.1103/PhysRevB.64.245202)
4. Boyd RW, Gauthier DJ, Gaeta AL, Willner AE. 2005 Maximum time delay achievable on propagation through a slow-light medium. *Phys. Rev. A* **71**, 023801. (doi:10.1103/PhysRevA.71.023801)
5. Podivilov E, Sturman B, Shumelyuk A, Odoulov S. 2003 Light pulse slowing down up to 0.025 cm/s by photorefractive two-wave coupling. *Phys. Rev. Lett.* **91**, 083902. (doi:10.1103/PhysRevLett.91.083902)
6. Ropers C *et al.* 2006 Ultrafast dynamics of surface plasmon polaritons in plasmonic metamaterials. *Appl. Phys. B* **84**, 183–189. (doi:10.1007/s00340-006-2191-4)
7. Ropers C, Park DJ, Stibenz G, Steinmeyer G, Kim J, Kim DS, Lienau C. 2005 Femtosecond light transmission and subradiant damping in plasmonic crystals. *Phys. Rev. Lett.* **94**, 113901. (doi:10.1103/PhysRevLett.94.113901)
8. Linden S, Kuhl J, Giessen H. 2001 Controlling the interaction between light and gold nanoparticles: selective supression of extinction. *Phys. Rev. Lett.* **86**, 4688–4691. (doi:10.1103/PhysRevLett.86.4688)
9. Christ A, Zentgraf T, Kuhl J, Tikhodeev SG, Gippius NA, Giessen H. 2004 Optical properties of planar metallic photonic crystal structures: experiment and theory. *Phys. Rev. B* **70**, 125113. (doi:10.1103/PhysRevB.70.125113)
10. Zentgraf T, Christ A, Kuhl J, Giessen H. 2004 Tailoring ultrafast dephasing of quasiparticles in metallic photonic crystals. *Phys. Rev. Lett.* **93**, 243901. (doi:10.1103/PhysRevLett.93.243901)
11. Christ A, Tikhodeev SG, Gippius NA, Kuhl J, Giessen H. 2003 Waveguide-plasmon polaritons: strong coupling of photonic and electronic resonances in a metallic photonic crystal slab. *Phys. Rev. Lett.* **91**, 183901. (doi:10.1103/PhysRevLett.91.183901)
12. Fleischhauer M, Imamoglu A, Marangos JP. 2005 Electromagnetically induced transparency: optics in coherent media. *Rev. Mod. Phys.* **77**, 633–673. (doi:10.1103/RevModPhys.77.633)
13. Zhang S, Genov D, Wang Y, Liu M, Zhang X. 2008 Plasmon-induced transparency in metamaterials. *Phys. Rev. Lett.* **101**, 047401. (doi:10.1103/PhysRevLett.101.047401)
14. Fan S, Suh W, Joannopoulos JD. 2003 Temporal coupled-mode theory for the Fano resonance in optical resonators. *J. Opt. Soc. Am. A* **20**, 569–572. (doi:10.1364/JOSAA.20.000569)
15. Dutton Z, Hau LV. 2004 Storing and processing optical information with ultraslow light in Bose-Einstein condensates. *Phys. Rev. A* **70**, 053831. (doi:10.1103/PhysRevA.70.053831)
16. Luk'yanchuk B, Zheludev NI, Maier SA, Halas NJ, Nordlander P, Giessen H, Chong CT. 2010 The Fano resonance in plasmonic nanostructures and metamaterials. *Nat. Mater.* **9**, 707–715. (doi:10.1038/nmat2810)
17. Miroshnichenko AE, Flach S, Kivshar YS. 2010 Fano resonances in nanoscale structures. *Rev. Mod. Phys.* **82**, 2257–2298. (doi:10.1103/RevModPhys.82.2257)
18. Brown DP, Walker MA, Urbas AM, Kildishev AV, Xiao S, Drachev VP. 2012 Direct measurement of group delay dispersion in metamagnetics for ultrafast pulse shaping. *Opt. Express* **20**, 23 082–23 087. (doi:10.1364/OE.20.023082)
19. Tikhodeev SG, Yablonskii AL, Muljarov EA, Gippius NA, Ishihara T. 2002 Quasiguided modes and optical properties of photonic crystal slabs. *Phys. Rev. B* **66**, 045102. (doi:10.1103/PhysRevB.66.045102)
20. Engheta N, Salandrino A, Alu A. 2005 Circuit elements at optical frequencies: nanoinductors, nanocapacitors, and nanoresistors. *Phys. Rev. Lett.* **95**, 095504. (doi:10.1103/PhysRevLett.95.095504)
21. Grigorenko AN, Geim AK, Gleeson HF, Zhang Y, Firsov AA, Khrushchev IY, Petrovic J. 2005 Nanofabricated media with negative permeability at visible frequencies. *Nature* **438**, 335–338. (doi:10.1038/nature04242)

22. Klein MW, Tritschler T, Wegener M, Linden S. 2005 Lineshape of harmonic generation by metallic nanoparticles and metallic photonic crystal slabs. *Phys. Rev. B* **72**, 115113. (doi:10.1103/PhysRevB.72.115113)
23. Linden S, Giessen H, Kuhl J. 1998 XFROG—a new method for amplitude and phase characterization of weak ultrashort pulses. *Phys. Stat. Sol. B* **206**, 119–124. (doi:10.1002/(SICI)1521-3951(199803)206:1<119::AID-PSSB119>3.0.CO;2-X)
24. Trebino R. 2000 *Frequency-resolved optical gating: the measurement of ultrashort laser pulses*. Dordrecht, The Netherlands: Kluwer Academic Publishers.
25. Dogariu A, Nahata A, Linke RA, Wang LJ, Trebino R. 2002 Optical pulse propagation through metallic nano-apertures. *Appl. Phys. B* **74**, s69–s73.(doi:10.1007/s00340-002-0910-z)
26. Ho KM, Chan CT, Soukoulis CM. 1990 Existence of a photonic gap in periodic dielectric structures. *Phys. Rev. B* **65**, 3152–3155. (doi:10.1103/PhysRevLett.65.3152)
27. Whittaker DM, Culshaw IS. 1999 Scattering-matrix treatment of patterned multilayer photonic structures. *Phys. Rev. B* **60**, 2610–2618. (doi:10.1103/PhysRevB.60.2610)
28. Genet C, van Exter MP, Woerdman JP. 2003 Fano-type interpretation of red shifts and red tails in hole array transmission spectra. *Opt. Commun.* **225**, 331–336. (doi:10.1016/j.optcom.2003.07.037)
29. Sarrazin M, Vigneron J-P, Vigoureux J-M. 2003 Role of Wood anomalies in optical properties of thin metallic films with a bidimensional array of subwavelength holes. *Phys. Rev. B* **67**, 085415. (doi:10.1103/PhysRevB.67.085415)
30. Johnson PB, Christy RW. 1972 Optical constants of the noble metals. *Phys. Rev. B* **6**, 4370–4379. (doi:10.1103/PhysRevB.6.4370)
31. Fan S, Joannopoulos JD. 2002 Analysis of guided resonances in photonic crystal slabs. *Phys. Rev. B* **65**, 235112. (doi:10.1103/PhysRevB.65.235112)
32. Gippius NA, Tikhodeev SG, Ishihara T. 2005 Optical properties of photonic crystal slabs with an asymmetrical unit cell. *Phys. Rev. B* **72**, 045138. (doi:10.1103/PhysRevB.72.045138)
33. Biyikli N, Kimukin I, Butun B, Aytür O, Ozbay E. 2004 ITO-Schottky photodiodes for high-performance detection in the UV-IR spectrum. *IEEE Sel. Top. Q. Electron.* **10**, 759–765. (doi:10.1109/JSTQE.2004.833977)

rsta.royalsocietypublishing.org *Phil. Trans. R. Soc. A* **375**: 20160065